Journal of Alloys and Compounds 693 (2017) 1243–1249

Contents lists available at ScienceDirect

Journal of Alloys and Compounds

journal homepage: http://www.elsevier.com/locate/jalcom

Micro far-infrared dielectric response of lanthanide orthotantalates for applications in microwave circuitry

Anderson Dias [a, *], Kisla P.F. Siqueira [a], Roberto L. Moreira [b]

[a] Departamento de Química, Universidade Federal de Ouro Preto, Campus Morro do Cruzeiro, ICEB II, Sala 67, 35400-000, Ouro Preto, MG, Brazil
[b] Departamento de Física, ICEx, UFMG, C.P. 702, 30123-970, Belo Horizonte, MG, Brazil

ARTICLE INFO

Article history:
Received 17 June 2016
Received in revised form
5 September 2016
Accepted 9 October 2016
Available online 13 October 2016

Keywords:
Ceramics
Infrared reflectivity
Rare earth
Microwave
Dielectric resonators
Orthotantalates

ABSTRACT

Lanthanide orthotantalates $LnTaO_4$ (Ln = La, Nd, Dy and Lu) were synthesized by solid-state reactions at 1300 °C leading to well crystallized single-phase materials. XRD and infrared spectroscopic investigations showed that the samples exhibited three different monoclinic crystal structures depending on the lanthanide ion: $P2_1/c$ (for La), I2/a (for Nd) and P2/a (for Dy and Lu). For $LaTaO_4$, 21 polar modes could be depicted from the unpolarized infrared reflectivity spectrum, while group theory tools foreseen 33 infrared-active modes – the absent mode are likely hidden by accidental degeneracy. The smaller lanthanides (Nd, Dy and Lu) exhibited all the 15 predicted infrared-active bands, in perfect agreement with group-theory calculations, despite the mixing of polarization symmetry due to the polycrystalline nature of the samples. The intrinsic (infrared) dielectric properties were determined for all samples indicating that these orthotantalate ceramics could be candidates for microwave (MW) circuitry applications. $LaTaO_4$ ceramics exhibited the best MW dielectric response among the investigated $LnTaO_4$ ($\varepsilon_r = 21.2$ and estimated $Q_u \times f \approx 77$ THz), followed by $DyTaO_4$ ($\varepsilon_r = 19.9$ and $Q_u \times f \approx 75$ THz), $NdTaO_4$ ($\varepsilon_r = 18.7$ and $Q_u \times f \approx 55$ THz), and $LuTaO_4$ ($\varepsilon_r = 16.2$ and $Q_u \times f \approx 60$ THz).

1. Introduction

Lanthanide orthotantalates have shown a broad range of applications such as phosphors for solid-state lighting, photocatalysts (either for contaminant degeneration or hydrogen production), chemically robust hosts for nuclear materials and wastes, ion conductors for lithium batteries or solid-oxide fuel cells etc [1–17]. These applications become possible because lanthanide orthotantalates present high chemical and electrochemical stabilities, photo-electronic activities [1–4], ion conductivities [5,6,17], and strong luminescence [7–14]. For the production of these materials, there exist many synthetic routes, including the well-known solid state reaction, as well as many others non-conventional procedures [18–21]. The large range of synthetic possibilities lead very often to the crystallization of polymorphs (depending on the lanthanide ionic radius and processing conditions), which, in consequence, promotes different structural assignments and controversies in the literature [19].

In the last decades, previous works recognized that larger lanthanide orthotantalates belong to monoclinic structures ($P2_1/c$), while materials containing intermediate and smaller lanthanides (Ln = Nd-Lu) present *fergusonite*-type structures, depending upon the employed processing conditions [22]. In this respect, a polymorphic transformation within the *fergusonite* group (M'-type→M-type) was studied by Markiv et al. [19] and the results showed that it occurs by a thermally activated process and at particular temperature and enough holding time (to allow structural rearrangement) [19]. In short, these three parameters (temperature, annealing time and ionic radius) define the atomic arrangement of the material. Vullum et al. [23] showed that under certain special conditions (that revealed to be difficult to be experimentally reproduced), the orthorhombic phases $A2_1am$ and *Pbca* can also be produced for larger lanthanide ions (La-Pr). Very recently, Siqueira et al. [24] reported the production of all the lanthanide orthotantalate series and described their crystal structures as functions of temperature, time and ionic radius. Conversely to the lanthanide orthoniobates, where only the monoclinic structure $C2/c$ was reported for all compositions [25], it was observed that the lanthanide orthotantalates exhibited three different crystal structures along the series. For the largest lanthanides ($LaTaO_4$ and $PrTaO_4$), the monoclinic structure $P2_1/c$ (C_{2h}^5,

* Corresponding author.
E-mail address: anderson_dias@iceb.ufop.br (A. Dias).

http://dx.doi.org/10.1016/j.jallcom.2016.10.077
0925-8388/

#14, Z = 4) could be assigned, while for the intermediate lanthanides ($NdTaO_4$ to $TbTaO_4$), the M-type *fergusonite* structure I2/a (C_{2h}^6, #15, Z = 4) was observed. Samples with the smallest ionic radii ($DyTaO_4$ to $LuTaO_4$) presented the M'-type *fergusonite* structure P2/a (C_{2h}^4, #13, Z = 2) [24].

It is well recognized that tantalum-based materials are the best candidates for potential applications in microwave (MW) circuitry, owing to their adequate dielectric merit factors in the MW range: high dielectric constants, high unloaded quality factors (Q_u) and low variation of the resonant frequencies with temperature (τ_f) [26]. These are crucially important requirements for a solid state component to be useful in MW devices like filters and oscillators used in the telecommunication industry. Among the Ta-based materials, $Ba(Mg_{1/3}Ta_{2/3})O_3$ has stimulated a surge of interest for its excellent dielectric properties in the *X*-band (8–12 GHz) and has been considered the archetypal high-*Q* dielectric resonator material [27–29]. Communication systems operating in the MW-frequency range require low-loss ($Q_u \times f > 20$ THz) and high dielectric constant ($\varepsilon_r > 20$) materials as basic components in oscillators, filters and antennas [27–29]. Such materials ensure better performance along with reduction of weight and overall dimensions of the MW devices [29]. However, as a general trend, by increasing the dielectric permittivity, Q_u decreases and τ_f increases [29,30]. Therefore, the development of MW ceramics with adequate dielectric properties for specific applications is a challenging problem in dielectric resonator materials research.

Vibrational studies of the crystal structures and phonon features by using infrared spectroscopy have been currently employed in materials to investigate the behavior of their polar modes, once these modes determine completely the intrinsic dielectric contributions to the MW response and are directly dependent on the crystalline structure. Thus, in order to study the potential of a given material to MW applications (resonators or filters), the knowledge of its polar phonon features is mandatory. Lanthanide-based materials were previously studied by Dias et al. [25,31–33] from the point of view of their intrinsic dielectric properties, where different cubic, tetragonal, orthorhombic, and monoclinic structures exhibit different MW dielectric properties. Focusing now on lanthanide orthotantalates, the purpose of the present paper is to report on the investigation of the infrared-reflectivity spectra and on the determination of the intrinsic dielectric properties of $LaTaO_4$ ($P2_1/c$), $NdTaO_4$ (I2/a) and (Dy,Lu)TaO_4 (P2/a) ceramics, considered as archetypal of the monoclinic structures found for the entire series of lanthanide orthotantalates [24]. At the best of our knowledge, the present results constitute the first determination of the infrared phonon modes and of the intrinsic dielectric response of lanthanide orthotantalates. The obtained far-infrared polar phonons besides mid-infrared features allowed us to discuss on the intrinsic properties that underlie the optical and dielectric applications of this series of compounds. In particular, the results show that lanthanide orthotantalates could be new promising materials for MW applications.

2. Experimental

$LnTaO_4$ powders were synthesized by using Ln_2O_3 (Ln = La, Nd, Dy, and Lu) and Ta_2O_5 (>99.9%, Sigma-Aldrich) as starting materials through solid-state reaction. Stoichiometric amounts were weighed and mixed with a mortar and pestle. The mixed powders were calcined at 1300 °C, for different times: 14 h (La), 9 h (Dy), and 6 h (Nd and Lu). Cylindrical pucks of about 5 mm height and 12.5 mm diameter were made by applying a pressure of 150 MPa, followed by sintering in a conventional oven for 4 h. All samples were characterized by X-ray diffraction (XRD) using a Shimadzu D-6000 diffractometer with graphite monochromator and a nickel filter in the range of 10–60°2θ (15 s/step of 0.02°2θ), operating with FeKα radiation ($\lambda = 0.1936$ nm), 40 kV and 20 mA (the results were automatically converted to CuKα radiation for data treatment and manipulation).

Infrared measurements were performed in a Fourier transform spectrometer (Nicolet Nexus 470), equipped with a Centaurus microscope (10 × magnification, incident lightbeam with 350 μm diameter). In its commercial configuration, designed only for mid-infrared measurements (550-4000 cm^{-1}), this spectrometer uses a SiC source, a KBr:Ge beamsplitter and a liquid-N_2-cooled HgCdTe (MCT) detector. Mid-infrared reflectivity spectra were obtained under nitrogen purge, by averaging at least 64 scans, using observation regions of 230 μm × 230 μm, with spectral resolution of 2 cm^{-1}. A gold mirror was used for the reference spectra. Due to the small measuring sample area, no polishing was required to the sample. The sample surfaces were plane and smooth enough in many regions within the observation area to give quite appropriate spectra.

In order to reach the far-infrared region, we have adapted the Centaurus microscope to receive a far-infrared detector and used an appropriate solid substrate Si-beamsplitter. In the Centaurus microscope, the incident (parallel) light beam is focused on the sample by a Cassegrain reflector (consisting of a primary concave mirror and a coaxial secondary convex mirror), which also collects the reflected light that, by its turn, is directed to the MCT detector by a set of five plane mirrors, followed by one parabolic focusing mirror. We have mounted the latest plane mirror on a removable holder, so that when it is positioned, the mid-infrared configuration is recovered. By removing this mirror, the infrared beam reaches the rear part of the microscope going out through a hole made in it. Then, an off-axis parabolic mirror (Melles-Griot, focal distance of 7.5 cm) mounted on a xyz-positioning system was placed behind the microscope to focus the beam on a liquid-He-cooled Si-bolometer (Infrared Associates). The external rear entrance of the spectrometer was used to receive the output signal of the bolometer. Far-infrared measurements (50-700 cm^{-1}) were performed using the Si-beamsplitter and the bolometer detector, by averaging 64 scans. All other experimental conditions were the same as used for mid-infrared measurements. The reflectivity spectra obtained in mid- and far-infrared regions matched well in the superposition region. The overall spectra (50-4000 cm^{-1}) were treated within the four-parameter semi-quantum oscillator model, discussed below.

3. Results and discussion

Fig. 1 presents the XRD patterns for the lanthanide orthotantalates studied in this work. XRD data for $LaTaO_4$, $NdTaO_4$, $DyTaO_4$ and $LuTaO_4$ were indexed according to the International Committee for Diffraction Data (ICDD) cards #72-1808, #33-0941, #24-0379 and #24-1263, respectively. Single-phase, crystalline ceramics were obtained after processing without contaminants or secondary phases. As it can be observed in Fig. 1, the samples exhibit three different crystal structures after processing. These three structures are directly related to the ionic radius of the rare-earth metals. For $LaTaO_4$, the ceramics crystallized within the monoclinic structure, $P2_1/c$ space group (C_{2h}^5, #14 and Z = 4), with lattice parameters $a = 7.701$ Å; $b = 5.561$ Å; $c = 8.122$ Å and $\beta = 103.7°$. This structure was firstly described by Cava and Roth [34] and is formed by noncoplanar arrays of oxygen ions with 8-fold coordinated tantalum ions.

For $NdTaO_4$, the observed structure corresponds to the M-type *fergusonite*, I2/a (C_{2h}^6, #15 and Z = 4), with lattice parameters $a = 5.516$ Å; $b = 11.246$ Å; $c = 5.116$ Å and $\beta = 95.7°$. This structure was described by Santoro et al. [35] and by Mather and Davies [36], consisting of a monoclinic distortion (sheared version) of the

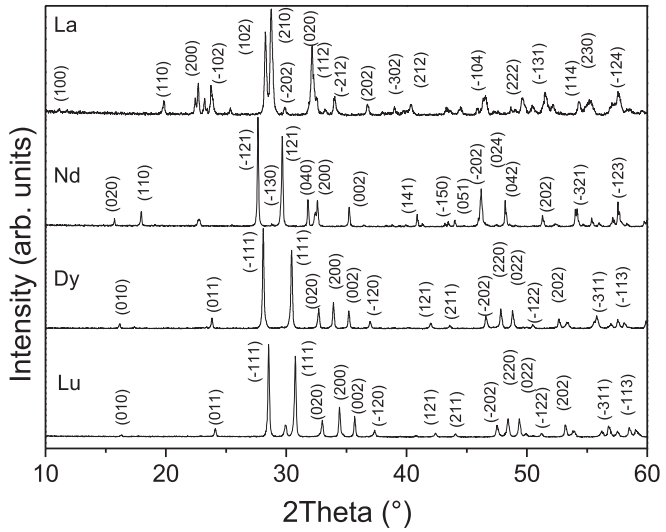

Fig. 1. XRD patterns for the $LaTaO_4$, $NdTaO_4$, $DyTaO_4$ and $LuTaO_4$ samples with the respective crystallographic planes, indexed by the ICDD cards #72-1808, #33-0941, #24-0379 and #24-1263, respectively.

tetragonal *scheelite* structure. In this configuration, Nd and Ta occupy different sites within separate layers to form a three dimensional cation-ordered structure. Tantalum ions approach six-fold coordination with the nearest neighbor oxygen ions arranged in a distorted tetragonal configuration [35,36]. Finally, $DyTaO_4$ and $LuTaO_4$ exhibited the M'-type *fergusonite* structure, belonging to the space group P2/a (C_{2h}^4, #13 and Z = 2). For $DyTaO_4$, the lattice parameters were $a = 5.289$ Å; $b = 5.472$ Å; $c = 5.101$ Å and $\beta = 92.7°$, while for $LuTaO_4$ the lattice parameters were $a = 5.237$ Å; $b = 5.424$ Å; $c = 5.058$ Å and $\beta = 96.1°$. This structure, which was described by Mather and Davies [36] and by Blasse et al. [37], contains TaO_6 octahedra with four shorter and two longer Ta-O distances (frequently indicated as TaO_6 centers). The rare earth ions are in 8-fold coordination sites (a distorted square antiprism) with C_2 site symmetry.

In the present work, the processing parameters are directly related to the final crystalline structures obtained. For example, Hartenbach et al. [21] synthesized lanthanide orthotantalates (La-Nd and Sm-Lu) by molten-salt processing at 1000 °C and found only two symmetries, namely $P2_1/c$ (La-Pr) and $P2/c$ (Nd, Sm-Lu). The differences between M-type (Nd) and M'-type (Dy, Lu) *fergusonite* structures are relatively small, but can be discerned by XRD techniques through careful analyses of the peaks around 18°2θ, 24°2θ, and 47°2θ. The (110) reflection peak is present only in the M-type structure (Nd at 18°2θ); also, the peak corresponding to the (011) plane is more intense in the M'-type structure (Dy, Lu at 24°2θ). The (−202), (024), and (042) reflections at around 47°2θ are closer in the M-type *fergusonite* structure (Nd), while their respective planes in the M'-type structure (Dy, Lu) are better resolved (see the (−202), (220), and (022) reflections).

Table 1 presents all relevant structural information required for the vibrational spectroscopic analyses, for the three different structures studied here: the occupied Wyckoff positions, the site symmetry and the phonons distribution at the Brillouin zone center in terms of the irreducible representations (determined from the nuclear site method developed by Rousseau et al. [38]). According to group-theory calculations presented in Table 1, there would be 33 infrared-active modes for $LaTaO_4$ ($17A_u \oplus 16B_u$) in the $P2_1/c$ space group, and 15 polar (infrared) bands predicted for $NdTaO_4$ ($7A_u \oplus 8B_u$) in the I2/a space group. Fifteen polar phonons are also expected for both members of the P2/a space group, $DyTaO_4$ and $LuTaO_4$, with $7A_u \oplus 8B_u$ symmetries.

Fourier-transform infrared spectroscopy was carried out at room temperature for all samples and the experimental spectra were adjusted within the four-parameter semi-quantum model [39], with a non-linear least-square program [40]. Within this model, the infrared phonon contribution of the N polar phonons to the complex dielectric dispersion function $\varepsilon(\omega)$, at a wavenumber ω, is given by:

$$\varepsilon(\omega) = \varepsilon_\infty \prod_{j=1}^{N} \frac{\Omega_{j,LO}^2 - \omega^2 + i\omega\gamma_{j,LO}}{\Omega_{j,TO}^2 - \omega^2 + i\omega\gamma_{j,TO}}, \quad (1)$$

where ε_∞ is the electronic polarization contribution, and $\Omega_{j,LO}(\Omega_{j,TO})$ and $\gamma_{j,LO}(\gamma_{j,TO})$ are the frequency and damping of the j-th longitudinal (transverse) optical polar modes, respectively. Indeed, the infrared dispersion originates from the strong interaction of the incident photons with the transverse optical (TO) vibrations of the crystal near the Brillouin zone center. Although the longitudinal

Table 1
Factor-group analysis for the three crystal structures assumed by the lanthanide orthotantalates sintered at 1300 °C.

Ceramics	Atom	Wyckoff sites	Symmetry	Irreducible representations
$LaTaO_4$	La	4*e*	C_1	$3A_g \oplus 3A_u \oplus 3B_g \oplus 3B_u$
$P2_1/c$	Ta	4*e*	C_1	$3A_g \oplus 3A_u \oplus 3B_g \oplus 3B_u$
	O (1)	4*e*	C_1	$3A_g \oplus 3A_u \oplus 3B_g \oplus 3B_u$
	O (2)	4*e*	C_1	$3A_g \oplus 3A_u \oplus 3B_g \oplus 3B_u$
	O (3)	4*e*	C_1	$3A_g \oplus 3A_u \oplus 3B_g \oplus 3B_u$
	O (4)	4*e*	C_1	$3A_g \oplus 3A_u \oplus 3B_g \oplus 3B_u$
$\Gamma_{TOTAL} = 18A_g \oplus 18B_g \oplus 18A_u \oplus 18B_u$, $\Gamma_{ACOUSTIC} = A_u \oplus 2B_u$				
$\Gamma_{RAMAN} = 18A_g \oplus 18B_g$ and $\mathbf{\Gamma_{INFRARED} = 17A_u \oplus 16B_u}$				
$NdTaO_4$	Nd	4*e*	C_2	$A_g \oplus A_u \oplus 2B_g \oplus 2B_u$
I2/a	Ta	4*e*	C_2	$A_g \oplus A_u \oplus 2B_g \oplus 2B_u$
	O (1)	8*f*	C_1	$3A_g \oplus 3A_u \oplus 3B_g \oplus 3B_u$
	O (2)	8*f*	C_1	$3A_g \oplus 3A_u \oplus 3B_g \oplus 3B_u$
$\Gamma_{TOTAL} = 8A_g \oplus 10B_g \oplus 8A_u \oplus 10B_u$, $\Gamma_{ACOUSTIC} = A_u \oplus 2B_u$				
$\Gamma_{RAMAN} = 8A_g \oplus 10B_g$ and $\mathbf{\Gamma_{INFRARED} = 7A_u \oplus 8B_u}$				
(Dy,Lu)TaO_4	Dy,Lu	2*f*	C_2	$A_g \oplus A_u \oplus 2B_g \oplus 2B_u$
P2/a	Ta	2*e*	C_2	$A_g \oplus A_u \oplus 2B_g \oplus 2B_u$
	O (1)	4*g*	C_1	$3A_g \oplus 3A_u \oplus 3B_g \oplus 3B_u$
	O (2)	4*g*	C_1	$3A_g \oplus 3A_u \oplus 3B_g \oplus 3B_u$
$\Gamma_{TOTAL} = 8A_g \oplus 10B_g \oplus 8A_u \oplus 10B_u$, $\Gamma_{ACOUSTIC} = A_u \oplus 2B_u$				
$\Gamma_{RAMAN} = 8A_g \oplus 10B_g$ and $\mathbf{\Gamma_{INFRARED} = 7A_u \oplus 8B_u}$				

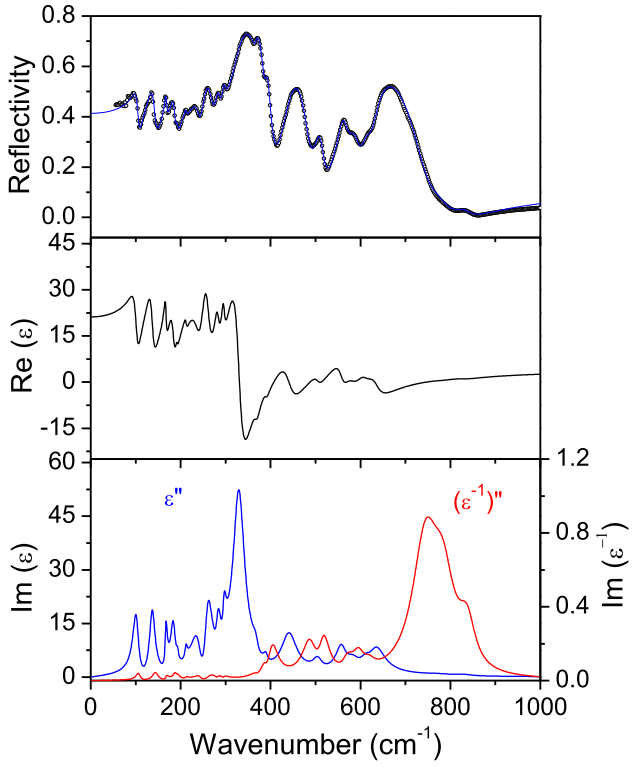

Fig. 2. Infrared experimental data and optical functions of $LaTaO_4$ sample. Top panel: reflectivity spectrum (black circles) and fitting curve (blue solid line). Optical functions obtained from the fitting of the infrared data are showed in middle and bottom panels: real part of the dielectric function (middle, black solid curve), imaginary part of the dielectric constant (ε") and imaginary part of the reciprocal dielectric constant (ε^{-1})" are in the bottom panel as blue and red solid curves, respectively. (For interpretation of the references to colour in this figure legend, the reader is referred to the web version of this article.)

Table 2
Dispersion parameters from the four parameters semi-quantum model adjust of the infrared reflectivity spectra of monoclinic $LaTaO_4$ ceramics. The wavenumbers (Ω) and damping constants (γ) are in cm^{-1}.

$\Omega_{j,TO}$	$\gamma_{j,TO}$	$\Omega_{j,LO}$	$\gamma_{j,LO}$	$\Delta\varepsilon_j$
102.0	15.5	106.9	11.3	2.390
136.8	15.4	144.0	15.6	2.126
167.0	5.6	168.5	7.4	0.361
183.8	11.9	187.7	11.1	0.803
193.0	5.3	193.5	5.7	0.061
212.0	6.4	212.5	6.9	0.100
241.2	27.9	243.1	15.7	0.578
259.7	22.3	271.9	23.3	2.330
282.9	11.8	286.0	16.5	0.335
296.0	8.3	296.7	12.0	0.101
329.6	31.6	367.9	17.2	4.854
368.5	13.7	388.3	14.8	0.046
389.8	11.4	403.0	29.0	0.034
441.1	42.2	487.9	37.0	1.048
505.3	24.2	517.9	27.5	0.137
558.6	26.3	568.9	26.7	0.322
583.7	42.0	596.9	27.9	0.293
610.5	34.1	620.0	31.0	0.224
633.0	41.1	744.1	71.4	0.423
775.0	65.0	786.0	58.0	0.022
832.0	49.0	839.0	45.0	0.021

$\varepsilon_\infty = 4.63$; $\varepsilon_r = 21.2$; $Q_u \times f \approx 77$ THz.

vibrations (LO) do not interact directly with the light, their corresponding frequencies appear explicitly in equation (1), which is quite convenient, once the LO-TO splitting determine the dielectric strengths. At low-incidence angles, the dielectric function is related to the optical reflectivity R by the Fresnel formula [39]:

$$R = \left|\frac{\sqrt{\varepsilon(\omega)} - 1}{\sqrt{\varepsilon(\omega)} + 1}\right|^2. \quad (2)$$

For $LaTaO_4$ ceramics, the reflectivity results are displayed in Fig. 2 (top panel) as black circles, along with the adjusted curves (solid blue line) obtained after fitting the experimental reflectivity data of the sample with eqs. (1) and (2). The optical functions obtained from those fittings are also presented in Fig. 2 (middle and bottom panels): real part of the dielectric function (ε'), imaginary of the dielectric function (ε"), and imaginary part of the reciprocal dielectric constant ($\eta = \varepsilon^{-1}$). The TO and LO frequencies of each polar mode can be determined from the poles and zeros of Re(ε), respectively, but the polar phonon characteristics (positions and widths) are more accurately determined from the peaks in Im(ε) and Im(η), for the TO and LO branches, respectively. Visual inspection of Fig. 2 shows, at least, 18 modes for $LaTaO_4$ spectra.

The obtained dispersion parameters for the TO and LO infrared branches for the $LaTaO_4$ ceramic are summarized in Table 2. It is worthy noticing that these oscillator parameters are indeed effective phonon parameters obtained by averaging the dielectric principal axes of the anisotropic polycrystalline sample, considered as formed by small grains in comparison with the infrared wavelengths. In such cases, for low-symmetry systems, the dielectric response is reduced (approximated) to that of a scalar, which is the average of the diagonal terms of the dielectric tensor [41]. We note that a total of 21 infrared modes could be discerned for this sample, in good agreement with the predicted modes for this monoclinic $P2_1/c$ structure. The infrared results presented here constitute the first determination of the polarized infrared modes for this lanthanum orthotantalate. For this material, the situation is quite similar to those of $LnMgB''O_6$ (Ln = lanthanide; B" = Ti, Sn) [42–44] and Ca_2MgTeO_6 [45] compounds, where quasi-accidental degeneracy forbids the distinction between A_u and B_u modes evolving correlated vibrations, and also only 17 infrared modes are observed instead of the 33 foreseen ones (also, $17A_u \oplus 16B_u$) [42–45]. It is worthy noticing the resemblance of the spectra of the $LaTaO_4$ and those of $LnMgB''O_6$ and Ca_2MgTeO_6, which derives from the fact that the vibrational modes come essentially from the MgO_6, $B''O_6$ and TeO_6 octahedra, as tentatively assigned in those cited references.

By knowing the phonon positions and widths, the phonon contributions to the dielectric function can be calculated. Indeed, the effective (averaged) dielectric strengths of the individual jth TO modes (presented in Table 2), can be obtained by the equation [39]:

$$\Delta\varepsilon_j = \frac{\varepsilon_\infty}{\Omega_{j,TO}^2} \times \frac{\prod_k \left(\Omega_{k,LO}^2 - \Omega_{j,TO}^2\right)}{\prod_{k\neq j} \left(\Omega_{k,TO}^2 - \Omega_{j,TO}^2\right)}. \quad (3)$$

The "static" dielectric constant in the microwave limit ($\Omega_{j,TO} >> \omega$) is obtained by adding the effective dielectric strengths:

$$\varepsilon_r = \varepsilon_\infty + \sum_{j=i}^{N} \Delta\varepsilon_j. \quad (4)$$

The values ofε_r, and ε_∞ are also listed in Table 2, beside the phonon dispersion parameters. The polar phonon dispersion parameters also allow us to estimate qualitatively the intrinsic unloaded quality factor Q_u extrapolated to the MW region ($\Omega_{j,TO} >> \omega$) [46], which is the reciprocal of the dielectric loss tangent($tan\ \delta$), given by

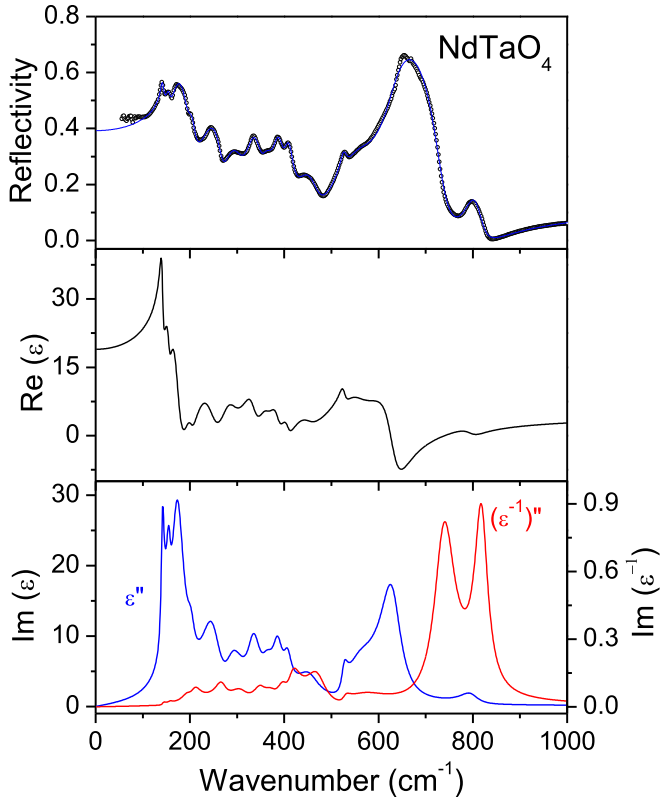

Fig. 3. Infrared experimental data and optical functions of $NdTaO_4$ sample. Top panel: reflectivity spectrum (black circles) and fitting curve (blue solid line). Optical functions obtained from the fitting of the infrared data are showed in middle and bottom panels: real part of the dielectric function (middle, black solid curve), imaginary part of the dielectric constant (ε ") and imaginary part of the reciprocal dielectric constant (ε^{-1})" are in the bottom panel as blue and red solid curves, respectively. (For interpretation of the references to colour in this figure legend, the reader is referred to the web version of this article.)

$$\tan\delta = \sum_j \tan\delta_j = \sum_j \omega \frac{\Delta\varepsilon_j \gamma_{j,TO}}{\varepsilon_r \Omega_{j,TO}^2}. \quad (5)$$

The estimated value for the quality factor extrapolated to 10 GHz ($Q_u \times$ f) is presented in Table 2. $LaTaO_4$ showed a qualitative intrinsic $Q_u \times$ f of about 77 THz, which is a good value if compared to other tantalum-based materials in ceramic form [29]. Indeed, the actual quality factor value could still be higher, but since we could not resolve all the infrared modes from the experimental spectrum of the $LaTaO_4$ ceramics, the fitted bandwidths were artificially overestimated, reducing their estimated quality factor.

Table 3
Dispersion parameters from the four parameters semi-quantum model adjust of the infrared reflectivity spectra of monoclinic $NdTaO_4$ ceramics. The wavenumbers (Ω) and damping constants (γ) are in cm^{-1}.

$\Omega_{j,TO}$	$\gamma_{j,TO}$	$\Omega_{j,LO}$	$\gamma_{j,LO}$	$\Delta\varepsilon_j$
141.8	7.5	143.5	9.5	0.844
156.0	11.5	157.5	10.9	0.809
174.4	34.6	196.2	29.0	5.269
203.0	19.3	209.1	24.5	0.328
250.5	56.3	268.3	28.1	2.276
287.2	50.0	311.1	48.5	1.296
334.1	33.4	351.6	30.3	0.730
360.4	28.2	370.3	42.2	0.187
385.8	23.5	396.8	28.4	0.259
407.0	19.3	415.9	31.6	0.127
451.2	56.2	471.1	51.0	0.390
526.3	15.3	528.4	19.3	0.071
548.8	71.0	563.6	110.0	0.357
630.5	52.4	738.2	52.7	1.128
796.3	45.9	818.7	33.8	0.078

$\varepsilon_\infty = 4.57$; $\varepsilon_r = 18.7$; $Q_u \times$ f ≈ 55 THz.

For $NdTaO_4$ ceramics, the reflectivity results are displayed in Fig. 3 (top panel) as black circles, along with the adjusted curves (solid blue line) obtained after fitting the experimental reflectivity data of the sample, as outlined above. The optical functions obtained from those fittings are also presented in Fig. 3 (middle and bottom panels): real part of the dielectric function (ε'), imaginary of the dielectric function (ε"), and imaginary part of the reciprocal dielectric constant ($\eta = \varepsilon^{-1}$). Again, the TO and LO branches of each polar mode (poles and zeros of Re(ε)) are clearly seen in the middle panel in Fig. 3. The phonon positions and widths are more accurately determined from the peaks in Im(ε) and Im(η), for the TO and LO branches, respectively. Visual inspection shows easily all the 15 predicted modes for $NdTaO_4$.

The obtained (adjusted) dispersion parameters for the TO and LO infrared branches for the $NdTaO_4$ sample are summarized in Table 3. We note that a total of 15 infrared modes could be discerned for this sample, in perfect agreement with the group-theory predictions for this monoclinic I2/a structure. By knowing the phonon positions and widths, the phonon contributions to the dielectric response were then calculated. The effective dielectric strengths for the individual jth TO modes ($\Delta\varepsilon_j$) were calculated (eq. (3), above), and the results are presented in Table 3. These dielectric strengths allow us to calculate the "static" dielectric constant (ε_r) in the microwave limit ($\Omega_{j,TO} >> \omega$) by adding all the $\Delta\varepsilon_j$, eq. (4), above. The values of ε_r, ε_∞ and of the qualitative $Q_u \times$ f (from equation (5)) are also given in Table 3. $NdTaO_4$ showed a qualitative intrinsic $Q_u \times$ f of about 55 THz (Table 3). This result can be interpreted as adequate for a tantalum-based material, being superior to many other ceramic systems well known as good MW resonators, including double perovskites [29].

For $DyTaO_4$ and $LuTaO_4$ ceramics, the reflectivity results are displayed in Fig. 4 as black circles, along with the adjusted curves (solid blue line for Dy, and solid red line for Lu) obtained after fitting the experimental reflectivity data of the sample with eqs. (1) and (2), as for the other materials studied in this work. As it can be seen, comparable results were obtained, as expected for materials

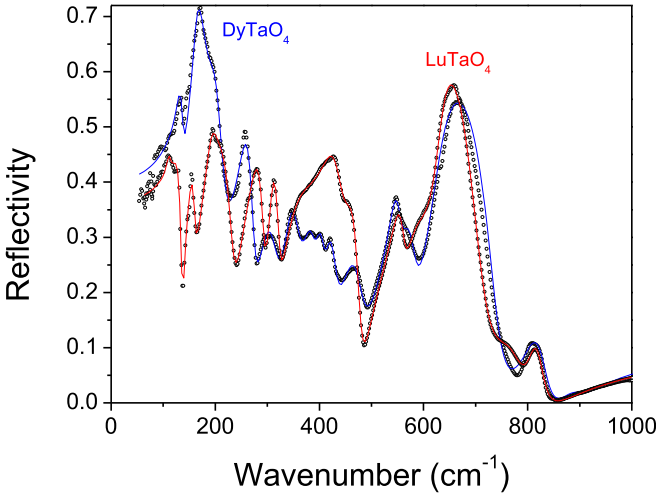

Fig. 4. Reflectivity spectra (black circles) and fitting curves (blue and solid lines) of $DyTaO_4$ and $LuTaO_4$ samples, respectively. (For interpretation of the references to colour in this figure legend, the reader is referred to the web version of this article.)

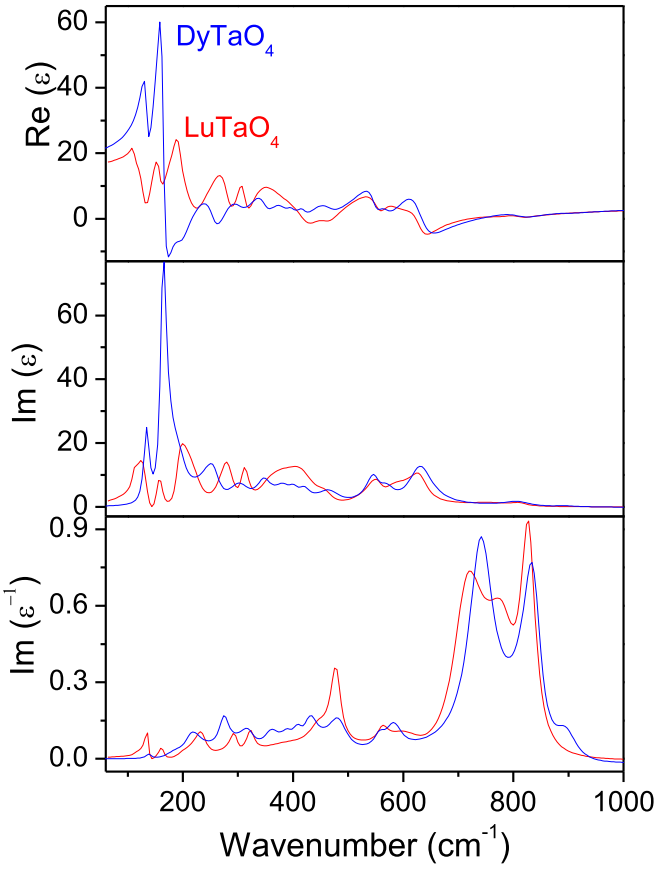

Fig. 5. Infrared optical functions for $DyTaO_4$ and $LuTaO_4$ samples. Top panel: real part of the dielectric function, Re (ε) (blue and red solid curves correspond to Dy and Lu, respectively). Middle panel: imaginary part of the dielectric constant, Im (ε). Bottom panel: imaginary part of the reciprocal dielectric constant, Im (ε^{-1}). (For interpretation of the references to colour in this figure legend, the reader is referred to the web version of this article.)

with the same crystal structure. Frequency shifts could be observed as a result of different ionic radii between Dy and Lu. The optical functions obtained from the experimental fittings are presented in Fig. 5 as blue and red solid curves, corresponding to $DyTaO_4$ and $LuTaO_4$, respectively. Top, middle and bottom panels exhibit the real part of the dielectric function, Re(ε), imaginary part of the dielectric function, Im (ε), and imaginary part of the reciprocal dielectric constant, Im (ε^{-1}). As it can be seen, both TO and LO branches of each polar mode, which represent the poles and zeros of Re(ε), are clearly seen in the top panel in Fig. 5. The phonon positions and widths are more accurately determined from the peaks in Im(ε) and Im (ε^{-1}), for the TO and LO branches, respectively. The visual inspection shows us at least 10 modes for both $DyTaO_4$ and $LuTaO_4$ spectra.

The fitting dispersion parameters for the TO and LO infrared branches for the $DyTaO_4$ and $LuTaO_4$ ceramics are summarized in Table 4 for both ceramics. We note that a total of 15 infrared modes could be discerned for these samples, in perfect agreement with the predicted modes for this monoclinic P2/a structure. The phonon contributions to the dielectric response were calculated and the values of ε_r, ε_∞ and $Q_u \times f$ are presented in Table 4, beside all phonon dispersion parameters. The overall phonon losses are presented in Table 4, where intrinsic $Q_u \times f$ values of about 75 THz and 60 THz were estimated for $DyTaO_4$ and $LuTaO_4$, respectively. According to Sebastian [29], a few ABO_4 compounds were studied by the literature owing to MW circuitry applications. Molybdates and

Table 4
Dispersion parameters from the four parameters semi-quantum model adjust of the infrared reflectivity spectra of monoclinic $DyTaO_4$ and $LuTaO_4$ ceramics. The wavenumbers (Ω) and damping constants (γ) are in cm^{-1}.

$\Omega_{j,TO}$	$\gamma_{j,TO}$	$\Omega_{j,LO}$	$\gamma_{j,LO}$	$\Delta\varepsilon_j$
134.0	12.0	138.0	12.0	2.043
163.5	14.0	181.2	42.9	5.230
195.7	37.1	215.2	33.4	1.678
258.0	36.3	274.4	21.1	1.462
303.8	49.8	319.8	35.0	0.974
346.9	32.8	360.7	33.4	0.658
383.3	34.1	391.3	24.3	0.404
400.1	23.1	408.7	23.4	0.237
419.9	23.5	430.1	29.3	0.199
465.9	51.5	484.0	41.5	0.449
547.5	28.3	556.1	23.6	0.428
568.1	37.0	583.8	34.9	0.326
630.1	53.0	741.0	53.0	1.043
810.6	62.0	837.3	39.7	0.108
892.0	50.0	897.0	50.0	0.018
$\varepsilon_\infty = 4.66$; $\varepsilon_r = 19.9$; $Q_u \times f \approx 75$ THz				
111.0	9.0	111.5	10.3	0.207
131.4	22.9	136.5	7.7	1.589
157.1	14.0	162.0	12.4	1.012
192.7	22.0	195.6	37.7	0.649
219.0	50.4	234.9	25.0	2.153
281.6	33.4	294.8	16.6	1.622
311.4	18.6	322.7	18.4	0.789
350.9	84.9	391.2	108.1	1.635
423.8	57.8	443.8	43.1	0.516
461.7	41.3	478.2	22.1	0.227
557.1	31.6	562.6	21.5	0.464
572.7	80.2	612.9	78.3	0.736
630.7	39.2	713.4	65.6	0.310
764.1	88.5	785.1	60.4	0.084
810.6	35.6	827.7	32.1	0.040
$\varepsilon_\infty = 4.18$; $\varepsilon_r = 16.2$; $Q_u \times f \approx 60$ THz.				

tungstates represent practically all the known electroceramics of this category, exhibiting *Scheelite* structure and being considered as "excellent dielectric materials" [29]. Their $Q_u \times f$ values of about 60–80 THz are in accordance with our results for lanthanide orthotantalates.

4. Conclusions

Lanthanide orthotantalates $LnTaO_4$ (Ln = La, Nd, Dy, and Lu) were synthesized by solid-state reactions in optimized conditions of temperature (1300 °C) and time (up to 14 h) to yield crystalline materials. The crystal structures of the obtained compounds were investigated by X-ray diffraction and all the samples exhibited monoclinic structures, but with different arrangements as a function of the ionic radius of the rare-earth metal. For compounds with the largest ionic radii (La), the ceramics crystallized in the monoclinic structure, $P2_1/c$ (C_{2h}^5, #14, Z = 4), while the compounds with intermediate ionic radii (Nd) exhibited the M-type *fergusonite* structure, I2/a (C_{2h}^6, #15, Z = 4). Samples with the smallest ionic radii (Dy and Lu) presented the M'-type *fergusonite* structure, P2/a (C_{2h}^4, #13, Z = 2). The infrared-reflectivity spectra and the polar phonon characteristics for these lanthanide orthotantalates are reported for the first time. A special experimental setup with an infrared microscope was implemented in order to obtain the far-infrared reflectivity spectra of these ceramics and allow the identification of the polar phonons foreseen for the material. The experimental results are in good agreement with our group theory predictions: $LaTaO_4$ sample with $P2_1/c$ (#14) group showed 21 infrared-active modes, while the all *Fergusonite* samples ($NdTaO_4$ with I2/a group and $DyTaO_4$ or $LuTaO_4$ with P2/a group) exhibited 15 infrared modes. Intrinsic dielectric properties were determined

and allowed us to present these orthotantalate ceramics as promising candidates for MW circuitry applications. In particular, $LaTaO_4$ exhibited the higher dielectric constant ($\varepsilon_r = 21.2$) and estimated $Q_u \times f \approx 77$ THz, followed by $DyTaO_4$ ($\varepsilon_r = 19.9$ and $Q_u \times f \approx 75$ THz), $NdTaO_4$ ($\varepsilon_r = 18.7$ and $Q_u \times f \approx 55$ THz), and $LuTaO_4$ ($\varepsilon_r = 16.2$ and $Q_u \times f \approx 60$ THz). These dielectric parameters are in the range of useful MW materials.

Acknowledgements

The authors acknowledge the financial support from CAPES, CNPq, FINEP and FAPEMIG.

References

[1] K. Shimizu, S. Itoh, T. Hatamachi, T. Kodama, M. Sato, K. Toda, Photocatalytic water splitting on Ni-intercalated Ruddlesden-popper tantalate $H_2La_{2/3}Ta_2O_7$, Chem. Mater. 17 (2005) 5161–5166.
[2] F.E. Osterloh, Inorganic materials as catalysts for photochemical splitting of water, Chem. Mater. 20 (2008) 35–54.
[3] R. Abe, M. Higashi, Z.G. Zou, K. Sayama, Y. Abe, H. Arakawa, Photocatalytic water splitting into H_2 and O_2 over R_3TaO_7 and R_3NbO_7 (R= Y, Yb, Gd, La): effect of crystal structure on photocatalytic activity, J. Phys. Chem. B 108 (2004) 811–814.
[4] M. Machida, J. Yabunaka, T. Kijima, Synthesis and photocatalytic property of layered perovskite tantalates, $RbLnTa_2O_7$ (Ln= La, Pr, Nd, and Sm), Chem. Mater. 12 (2000) 812–817.
[5] R. Haugsrud, T. Norby, Proton conduction in rare-earth ortho-niobates and ortho-tantalates, Nat. Mater. 5 (2006) 193–196.
[6] T. Mokkelbost, Ø. Andersen, R.A. Strom, K. Wiik, T. Grande, M. Einarsrud, High-temperature proton-conducting $LaNbO_4$-based materials: powder synthesis by spray pyrolysis, J. Am. Ceram. Soc. 90 (2007) 3395–3400.
[7] H. Zhang, Y. Wang, L. Xie, Luminescent properties of Tb^{3+} activated $GdTaO_4$ with M and M′ type structure under UV–VUV excitation, J. Lumin 130 (2010) 2089–2092.
[8] T. Pang, W. Cao, Y. Fu, X. Luo, Up-conversion luminescence of trivalent-rare-earth ion-doped $LnTaO_4$ (Ln= Y, Gd, La), Mater. Lett. 62 (2008) 2500–2502.
[9] W. Liu, Q. Zhang, L. Ding, D. Sun, J. Luo, S. Yin, Photoluminescence properties of $LuTaO_4:RE^{3+}$ ($RE^{3+} = Eu^{3+}$, Tb^{3+}) with m′-type structure, J. Alloys. Compd. 474 (2009) 226–228.
[10] B. Li, Z. Gu, J. Lin, M.Z. Su, Photoluminescence of Eu^{3+}-activated $GdTaO_4$ with both M Type and M′ type structures, J. Mater. Sci. 35 (2000) 1139–1143.
[11] B. Li, Z. Gu, J. Lin, M.Z. Su, X-ray luminescence properties of rare-earth doped orthotantalate, Mater. Res. Bull. 35 (2000) 1921–1931.
[12] B. Liu, K. Han, X. Liu, M. Gu, S. Huang, C. Ni, Z. Qi, G. Zhang, Luminescent properties of $GdTaO_4$ and $GdTaO_4:Eu^{3+}$ under VUV–UV excitation, Solid State Commun. 144 (2007) 484–487.
[13] W. Liu, Q. Zhang, W. Zhou, C. Gu, S. Yin, Growth and luminescence of m-type and Tb: scintillation single crystals, IEEE Trans. Nucl. Sci. 57 (2010) 1287–1290.
[14] I. Arellano, M. Nazarov, C.C. Byeon, E.J. Popovici, H. Kim, H.C. Kang, D.Y. Noh, Luminescence and structural properties of $Y(Ta,Nb)O_4:Eu^{3+}$, Tb^{3+} phosphors, Mater. Chem. Phys. 119 (2010) 48–51.
[15] M. Nyman, M.A. Rodriguez, L.E.S. Rohwer, J.E. Martin, M. Waller, F.E. Osterloh, Unique $LaTaO_4$ polymorph for multiple energy applications, Chem. Mater. 21 (2009) 4731–4737.
[16] T.Z. Forbes, M. Nyman, M.A. Rodriguez, A. Navrotsky, The energetics of lanthanum tantalate materials, J. Sol. State Chem. 183 (2010) 2516–2521.
[17] R. Haugsrud, T. Norby, High-temperature proton conductivity in acceptor-substituted rare-earth ortho-tantalates, $LnTaO_4$, J. Am. Ceram. Soc. 90 (2007) 1116–1121.
[18] M. Nyman, M.A. Rodriguez, T.M. Alam, T.M. Anderson, A. Ambrosini, Aqueous synthesis and structural comparison of rare earth niobates and Tantalates:$(La, K,¤)_2Nb_2O_{7-x}(OH)_2$ and $Ln_2Ta_2O_7(OH)_2$ (¤= vacancy; Ln= La–Sm), Chem. Mater 21 (2009) 2201–2208.
[19] V.Y. Markiv, N.M. Belyavina, Y.A. Titov, A.M. Sych, A.N. Sokolov, A.A. Kapshuk, M.S. Slobodyanyk, Peculiarities of polymorphic transformations in $YbTaO_4$ and crystal structure of its modifications, J. Alloys. Compd. 346 (2002) 263–268.
[20] V.V. Molchanov, M.G. Zuev, L.M. Plyasova, S.V. Bogdanov, Mechanochemical synthesis of Yttrium and lanthanum tantalates, Inorg. Mater. 40 (2004) 73–79.
[21] I. Hartenbach, F. Lissner, T. Nikelski, S.F. Meier, H.M.B. Bunz, T.Z. Schleid, About lanthanide oxotantalates with the formula $MTaO_4$ (M= La-Nd, Sm-Lu), Anorg. Allg. Chem. 631 (2005) 2377–2382.
[22] Y.A. Titov, A.M. Sych, A.N. Sokolov, A.A. Kapshuk, V.Y. Markiv, N.M. Belyavina, Crystal structure of the high-pressure modification of $NdTaO_4$, J. Alloys. Compd. 311 (2000) 252–255.
[23] F. Vullum, F. Nitsche, S.M. Selbach, T. Grande, Solid solubility and phase transitions in the system $LaNb_{1-x}Ta_xO_4$, J. Sol. State Chem. 181 (2008) 2580–2585.
[24] K.F.P. Siqueira, G.B. Carvalho, A. Dias, Influence of the processing conditions and chemical environment on the crystal structures and phonon modes of lanthanide orthotantalates, Dalton Trans. 40 (2011) 9454–9460.
[25] K.F.P. Siqueira, R.L. Moreira, A. Dias, Synthesis and crystal structure of lanthanide orthoniobates studied by vibrational spectroscopy, Chem. Mater. 22 (2010) 2668–2674.
[26] G. Subramanyam, M.W. Cole, N.X. Sun, T.S. Kalkur, N.M. Sbrockey, G.S. Tompa, X. Guo, C. Chen, S.P. Alpay, G.A. Rossetti Jr., K. Dayal, L.Q. Chen, D.G. Schlom, Challenges and opportunities for multi-functional oxide thin films for voltage tunable radio frequency/microwave components, J. Appl. Phys. 114 (2013) 191301.
[27] X. Zhang, L.C. Sengupta, E.A. Underhill, Tunable low loss material compositions and methods of manufacture and use therefore. U.S. Patent Application No. 12/286,841.
[28] L.Sengupta, Phased array antenna systems; capacitor/varistor protection devices; multilayer capacitors; nonvolatile computer memory; Low Loss Tangent and Threshold Voltage; High Nonlinear Voltage and Tunability. U.S. Patent No. 5,635,433. 3 Jun. 1997.
[29] M.T. Sebastian, Dielectric Materials for Wireless Communication, Elsevier, 2008.
[30] P.L. Wise, I.M. Reaney, W.E. Lee, D.M. Iddles, D.S. Cannell, T.J. Price, Tunability of τ_f in perovskites and related compounds, J. Mater. Res. 17 (2002) 2033–2040.
[31] R.L. Moreira, R.P.S. Lobo, G. Subodh, M.T. Sebastian, F.M. Matinaga, A. Dias, Optical phonon modes and dielectric behavior of $Sr_{1-3\ x/2}Ce_xTiO_3$ microwave ceramics. Chem, Mater 19 (2007) 6548–6554.
[32] A. Dias, M.M. Lage, L.A. Khalam, M.T. Sebastian, R.L. Moreira, Vibrational spectroscopy of Ca_2LnTaO_6 (Ln= lanthanides, Y, and in) and Ca_2InNbO_6 double perovskites, Chem. Mater. 23 (2010) 14–20.
[33] A. Dias, L.A. Khalam, M.T. Sebastian, M.M. Lage, F.M. Matinaga, R.L. Moreira, Raman scattering and infrared spectroscopy of chemically substituted Sr_2LnTaO_6 (Ln= lanthanides, Y, and in) double perovskites, Chem. Mater. 20 (2008) 5253–5259.
[34] R.J. Cava, R.S. Roth, The structure of $LaTaO_4$ at 300° C by neutron powder profile analysis, J. Solid State Chem. 36 (1981) 139–147.
[35] A. Santoro, M. Marezio, R.S. Roth, D. Minor, Neutron powder diffraction study of the structures of $CeTaO_4$, $CeNbO_4$, and $NdTaO_4$, J. Solid State Chem. 35 (1980) 167–175.
[36] S.A. Mather, P.K. Davies, Nonequilibrium phase formation in oxides prepared at low temperature: fergusonite-related phases, J. Am. Ceram. Soc. 78 (1995) 2737–2745.
[37] G. Blasse, G.J. Dirksen, L.H. Brixner, M.K. Crawford, Luminescence of materials based on $LuTaO_4$, J. Alloys. Compd. 209 (1994) 1–6.
[38] D.L. Rousseau, R.P. Bauman, S.P.S. Porto, Normal mode determination in crystals, J. Raman Spectrosc. 10 (1981) 253–290.
[39] F. Gervais, P. Echegut, in: R. Blinc, A.P. Levanyuk (Eds.), Incommensurate Phases in Dielectrics, 1986, p. 337. North Holland, Amsterdam.
[40] D.D. Meneses, G. Gruener, M. Malki, P. Echegut, Causal voigt profile for modeling reflectivity spectra of glasses, J. Non-Cryst. Solids 351 (2005) 124–129.
[41] T.G. Mayerhöfer, J. Popp, Employing spectra of polycrystalline materials for the verification of optical constants obtained from corresponding low-symmetry crystals, Appl. Opt. 46 (2007) 327–334.
[42] A.N. Salak, D.D. Khalyavin, V.M. Ferreira, J.L. Ribeiro, L.G. Vieira, Structure refinement, far infrared spectroscopy, and dielectric characterization of $(1-x)La(Mg_{1/2}Ti_{1/2})O_3-xLa_{2/3}TiO_3$ solid solutions, J. Appl. Phys. 99 (2006) 094104.
[43] G.S. Babu, V. Subramanian, V.R.K. Murthy, I.N. Lin, C.T. Chia, H.L. Liu, Far-infrared, Raman spectroscopy, and microwave dielectric properties of $La(Mg_{0.5}Ti_{(0.5-x)}Sn_x)O_3$ ceramics, J. Appl. Phys. 102 (2007) 064906.
[44] G.S. Babu, V. Subramanian, V.R.K. Murthy, R.L. Moreira, R.P.S. Lobo, Crystal structure, Raman spectroscopy, far-infrared, and microwave dielectric properties of $(1-x)La(MgSn)_{0.5}O_3-xNd(MgSn)_{0.5}O_3$ system, J. Appl. Phys. 103 (2008) 084104.
[45] A. Dias, G. Subodh, G.M.T. Sebastian, M.M. Lage, R.L. Moreira, Vibrational studies and microwave dielectric properties of a-site-substituted tellurium-based double perovskites, Chem. Mater. 20 (2008) 4347–4355.
[46] J. Petzelt, S. Kamba, Submillimetre and infrared response of microwave materials: extrapolation to microwave properties, Mater. Chem. Phys. 79 (2003) 175–180.